УДК 528.8 DOI: https://doi.org/10.24028/gj.v47i5.333289

Spatiotemporal analysis of surface temperature dynamics in the Supii River basin using regression methods

S.V. Marhes, V.Ye. Filipovych, M.S. Lubskyi, 2025

Scientific Centre for Aerospace Research of the Earth of the Institute of Geological Sciences of the National Academy of Sciences of Ukraine, Kyiv, Ukraine
Received 22 June 2025

The research presents an approach for detecting spatial and temporal changes, specifically the annual increase in land surface temperature. The study area encompasses the Supii River basin, which spans the Chernihiv, Kyiv, and Cherkasy oblasts and flows into the Dnipro. This region is characterized by intensive agriculture, poor aquifer recharge, low-quality groundwater, and prolonged droughts.

Temperature data for July and August were obtained from publicly available Landsat mission archives for the period 1984—2024. It is recommended to recalculate Landsat thermal images based on emissivity, since their Level 2 product may contain pixels with missing information. To ensure the highest accuracy, pixels affected by clouds and their shadows were masked; the next stepinvolved time series analysis of the filtered images.

The time series analysis aimed to identify key patterns in the evolution of temperature dynamics, functionally dependent on various influencing factors. Accurate spatial alignment of the imagery enabled consistent undistorted calculation of the ground's physical characteristics over the entire study area and for each year of observation. A simple linear regression was applied to each pixel in each raster image. To visualize the spatial distribution of long-term temperature dynamics, the regression gradient (or slope coefficient) was used, representing the average annual increase in temperature.

The results are presented as spatial indices of annual surface temperature growth within the Supii River basin, highlighting settlements with dominant positive trends, and the distribution by land use cover. This provides insight into where and to what extent climate conditions may become critical in the coming years, assuming the temperature continues to rise. As a mitigation measure, it is proposed to vegetate the urban and rural areas (particularly in larger local communities) to help reduce the impact of global warming.

Key words: linear regression, time series, land surface temperature, annual increment, global warming.

Introduction. Against the backdrop of global environmental change driven by both climatic and anthropogenic forces, monitoring land surface temperature (LST) has become a crucial task in understanding geohydrological dynamics and ensuring sustainable water management at the river basin scale. LST functions as a fundamental environmental indicator that reflects changes in water availability, soil moisture, and vegetation health — parameters critical to ecosystem resilience.

Remote sensing (RS) technologies, particularly in combination with geospatial and statistical tools, offer a robust framework for analyzing spatial and temporal variations in surface temperature. Regression-based approaches, unlike traditional index-based methods (e.g., NDVI-LST correlations), enable the quantification of long-term trends

Citation: Marhes, S.V., Filipovych, V.Ye., & Lubskyi, M.S. (2025). Spatiotemporal analysis of surface temperature dynamics in the Supii River basin using regression methods. *Geofizychnyi Zhurnal*, *47*(5), 82—94. https://doi.org/10.24028/gj.v47i5.333289.

and provide statistically grounded interpretations of LST changes across heterogeneous landscapes [Bala et al., 2018; Li et al., 2018]. These models are instrumental in detecting subtle but consistent thermal trends, which often go unnoticed in simpler time-series comparisons.

The analytical foundations for such regression models lie not only in environmental statistics but also in classical linear algebra, which underpins the least-squares solutions, matrix-based operations, and model optimization [Cohn, 1994]. Foundational contributions to regression and time-series analysis [Draper, Smith, 1998; Chatfield, 2000; Brockwell, Davis, 2002] have further advanced these methodologies while smoothing techniques [Bowman, Azzalini, 1997] have improved the analysis of noisy temporal patterns. Recent studies confirm the efficacy of spatially distributed regression in LST modeling across various environmental contexts [Zhang, Li, 2020; Ismaila et al., 2023].

However, limited research has examined long-term LST dynamics at the basin scale in Eastern Europe using dense time series and pixel-wise regression approaches. Furthermore, few studies have integrated national methodologies with globally recognized statistical frameworks for spatial trend detection in heterogeneous rural-urban environments.

This study applies those analytical foundations to the Supii River basin, located in Ukraine's Left-Bank Forest-Steppe zone, which spans Chernihiv, Kyiv, and Cherkasy oblasts [Management…, 2021]. The basin is a mixed land-use environment where agricultural intensification, wetland degradation, and limited groundwater recharge converge, making it a relevant case for studying land-climate interactions.

This research aims to assess long-term spatial and temporal LST dynamics in the Supii River basin (1984—2024) using pixel-wise linear regression not previously applied in this region. Particular emphasis is placed on identifying local warming trends and the environmental conditions driving them. The study also integrates approaches developed by the Centre for Aerospace Research of the Earth (IGS NASU), which offer scalable solutions for thermal trend assessment [Stankevich et al., 2015; Lyalko et al., 2016; Filipovych, Shevchuk, 2018]. By focusing on annual temperature increases and pixel-level analysis over a multi-decadal period, the study addresses an

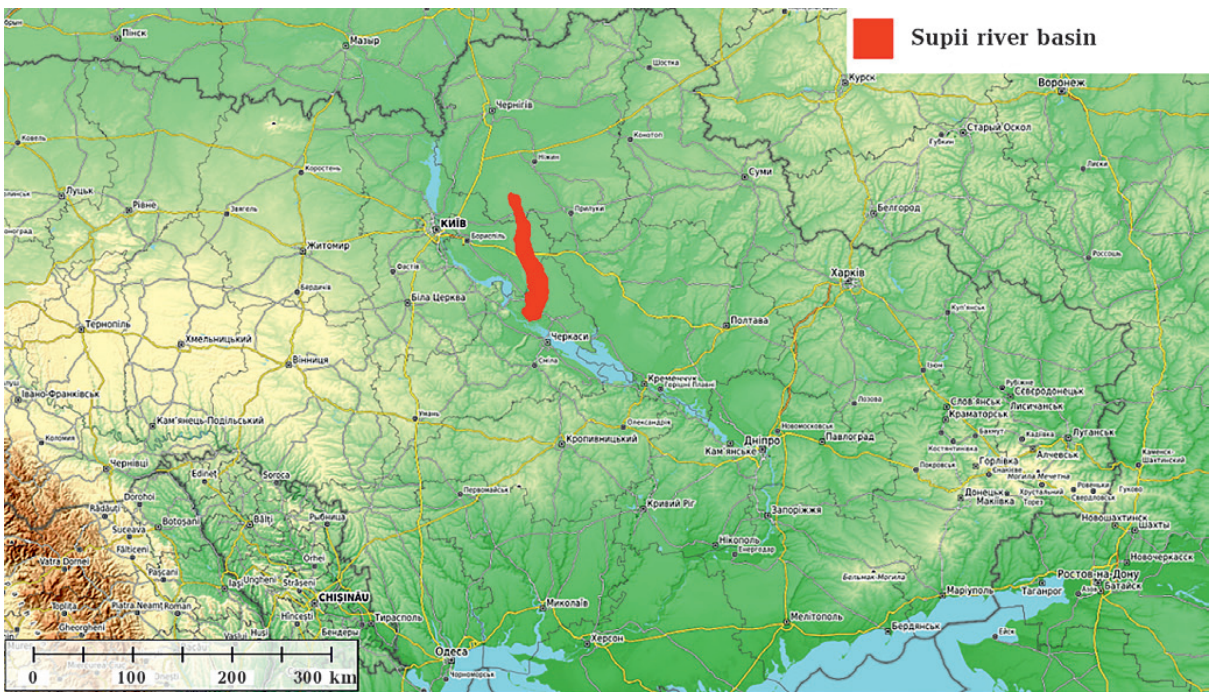

Fig. 1. Study area location.

important research gap and supports regional adaptation and land-use planning efforts.

The analysis enables a nuanced understanding of local warming processes, agroecological changes, and anthropogenic drivers of land surface temperature trends.

Study Area, Data and Methods. The Supii River, a left-bank tributary of the Dnipro River, flows for approximately 130—144 km with a basin area of around 2,000—2,165 km^2 (Fig. 1). It originates in swampy lowlands near Svydovets in the Nizhyn district (Chernihiv oblast) and flows through the Dnipro-Donetsk Depression and the foothills of the Ukrainian Crystalline Shield.

The valley ranges from 1.3 to 3.5 km in width. It contains two primary terrace levels: a marshy floodplain and the first supra-floodplain terrace. The floodplain, 0.5—1.0 m above river level, consists mainly of peat and peaty soils, with peaty sands and loams near the valley slopes. Channel widths vary from 2 to 8 m upstream to 20 m downstream. The basin comprises a heterogeneous landscape of wetlands, peatlands, and agricultural areas that collectively influence its hydrological dynamics [Derii, 2007].

The Supii basin provides essential ecosystem services: moisture and temperature regulation, biodiversity support, water purification through peat soils, and carbon sequestration. However, decades of intensive agriculture, drainage, and climate warming have degraded peatlands, reduced groundwater recharge, and increased fire risk due to flammable surfaces and dry periods [Lischenko et al., 2022].

Limited aquifer recharge, groundwater quality, and diffuse agricultural pollution further threaten the basin's ecological balance. These pressures highlight the need for integrated watershed management and hydrological restoration to sustain ecosystem functions and support regional climate adaptation goals. In this context, temperature emerges as one of the key determinants of the region's environmental sustainability, influencing hydrological processes, biological productivity, and the resilience of ecosystems to climatic and anthropogenic stressors, which necessitates its detailed spatial and temporal analysis.

The LST is determined from a thermal band of the Landsat satellite imagery series (10.6—12.5 μm). The series has been available since 1984 with a spatial resolution of 100 m, depending on the sensor, and is interpolated to 30 m, which corresponds to the visible and near-infrared channels. The temperature is determined using Planck's law adapted for Landsat satellites [Chander et al., 2009]:

$$T = \frac{K_2}{\ln\left(\frac{K_1}{L_s} + 1\right)}, \qquad (1)$$

where T is the LST (K); L_s is the land surface spectral radiance in thermal range after atmospheric correction, K_1 and K_2 are the constants for adapting Planck's law to the Landsat data.

For a precise estimate, it is necessary to enter the radiance data into the equation, considering the atmospheric influence and the land surface thermal emissivity. The following correction model is used [Yu et al., 2014]:

$$L_s = \frac{L_i - L_i^{\uparrow}}{\varepsilon_i \tau_i} - \frac{1 - \varepsilon_i}{\varepsilon_i} L_i^{\downarrow}, \qquad (2)$$

where L_i — top-of-atmosphere radiance in spectral range i; $L_i^{\uparrow}$, $L_i^{\downarrow}$, τ_i — parameters of the atmospheric influence on thermal radiation provided with satellite dataset; ε_i — land surface emissivity in spectral range i.

Next, the obtained radiance values are included in the Planck equation for temperature determination. The calculation of land surface temperature distribution is implemented in the Google Earth Engine geospatial data processing environment. The Landsat Level 2 Collection 2 product is provided with all the necessary parameters for data correction, allowing for the accurate retrieval of temperature distribution data. However, the reflectance model, which is represented by the ASTER Global Emissivity Dataset product, has significant disadvantages:

– relatively low spatial resolution (90 m);
– low update frequency (once every few months), which can significantly affect the resulting temperature;
– clouds could cover and mask part of the

studied area, which prevents the temperature from being obtained for this part of the studied surface.

Therefore, we applied the method of Valor and Caselles [1996] to derive the spatial distribution of surface emissivity from the relationship between emissivity and the normalized difference vegetation index (NDVI) for natural surfaces. This approach was implemented separately for bare soils (NDVI< –0.1) and for vegetated areas (NDVI>0.25). The surfaces with an emissivity within –0.1< NDVI<0.25correspond to artificial surfaces of towns and villages (asphalt, metal, and rubber covers, etc.) in the river valley. For them, emissivity is estimated by comparing the NDVI and emissivity according to ASTER GED geospatial product for 34 control points *via* the following dependence [Lubskyi et al., 2025]:

$$Em = 6.6972\left(\mathrm{NDVI}^3\right) - 2.2252\left(\mathrm{NDVI}^2\right) + \\ +0.1569\left(\mathrm{NDVI}\right) + 0.9586\,, \qquad (3)$$

where *Em* is the thermal emissivity at a particular point.

For equation (3), NDVI is calculated using Landsat optical data with a spatial resolution of 30 m, taken from the same image used for temperature estimation. Therefore, this approach enables both the removal of cloud masks from hidden areas in the ASTER GED data by incorporating cloud-free imagery and the acquisition of much more detailed temperature images. Fig. 2 illustrates the difference between the ASTER GED data and the NDVI-based emissivity derived from the Landsat image.

The resulting emissivity distribution is included in the Planck equation, adapted to the corresponding Landsat satellite data. A comparison of the baseline and resulting temperature images is presented in Fig. 3.

Thus, a LST time series was generated and used for regression analysis. All datasets underwent atmospheric and geometric corrections within the Google Earth Engine environment, after which the platform provided fully processed, analysis-ready images. These outputs were then processed in Python, where regression analysis produced temperature

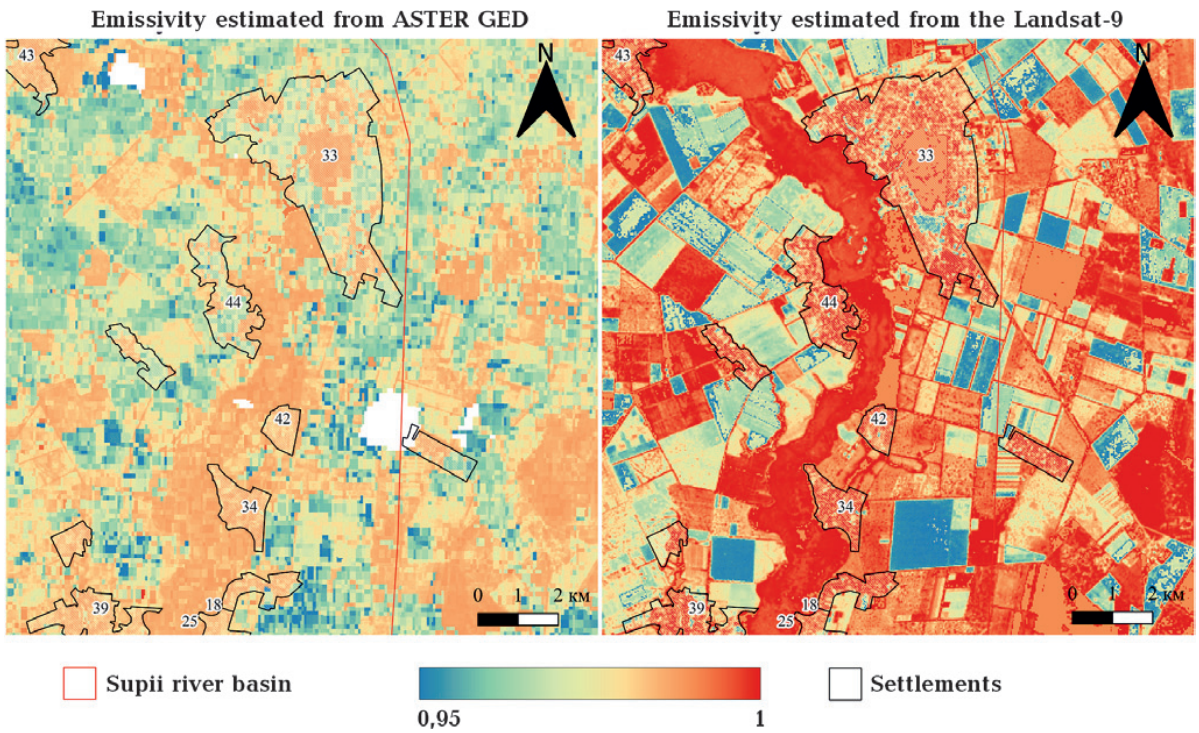

Fig. 2. Comparision between the ASTER GED emissivity data (masked areas are shown by red ellipses) at (left) and emissivity estimated from the Landsat-9 satellite data for August 21 2024 (the right part) for the Supii River near Zhurivka town.

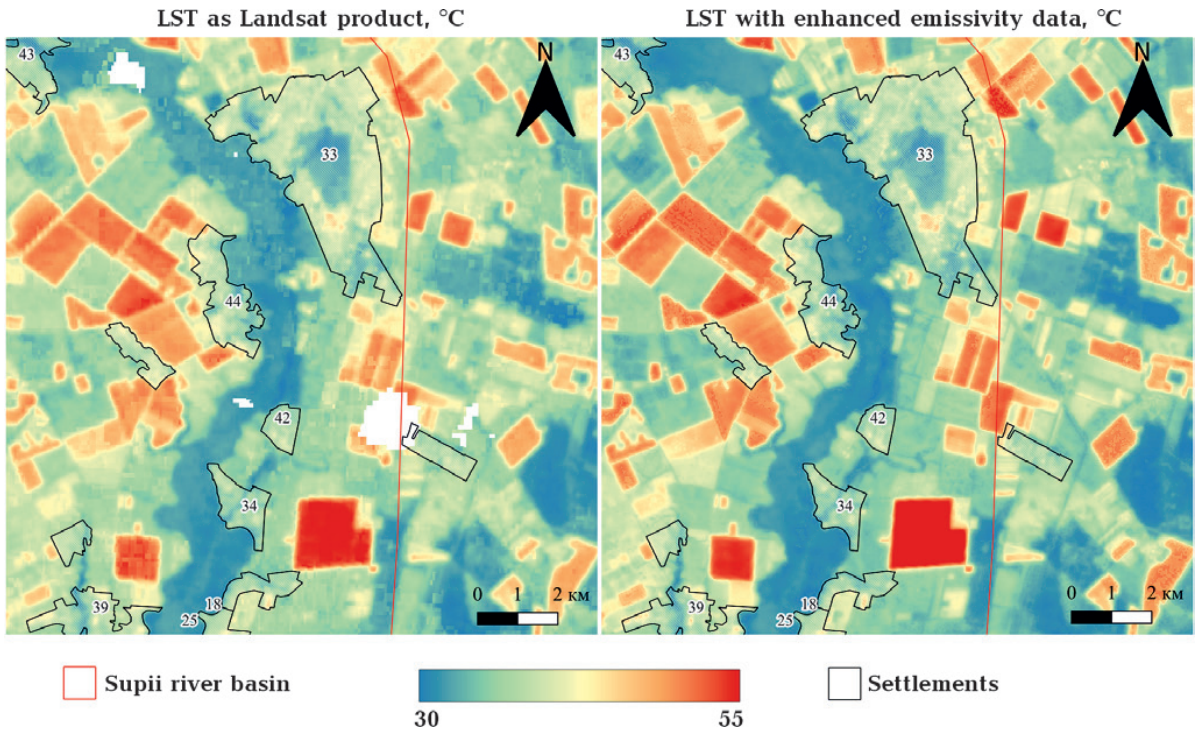

Fig. 3. Comparision between basic LST provided with Landsat-8 satellite geospatial product for August 20, 2024 (left) and the LST with enhanced emissivity data (right) for the the Supii River near Zhurivka town.

Table 1. Increase in mean land surface temperature in settlements along the Supii River since 1984

Settlement	LST_{max}	LST_{mean} (sorted)+SD	LST_{min}	RANGE
Zhurivka	0.392	0.112±0.129	0.000	0.392
Petrivka	0.354	0.121±0.125	–0.137	0.491
Tashan	0.268	0.177±0.045	0.017	0.251
Horbani	0.288	0.183±0.056	–0.007	0.295
Nekhaiky	0.308	0.184±0.056	–0.018	0.326
Farbovane	0.359	0.196±0.067	–0.150	0.509
Svydovets	0.307	0.207±0.050	–0.018	0.325
Voronky	0.365	0.213±0.058	–0.066	0.431
Demky	0.347	0.213±0.056	0.043	0.304
Nychyporivka	0.348	0.217±0.052	–0.006	0.355
Vepryk	0.362	0.219±0.051	0.027	0.336
Kapustyntsi	0.368	0.224±0.055	–0.007	0.375
Bezpalche	0.402	0.227±0.058	0.053	0.349
Novyi Bykiv	0.369	0.229±0.073	–0.077	0.445
Bezborodky	0.483	0.234±0.056	0.067	0.415
Yahotyn	0.501	0.244±0.054	–0.133	0.634
Helmiaziv	0.374	0.244±0.047	–0.044	0.418
Pishchane	0.537	0.250±0.060	–0.018	0.554
Kozatske	0.479	0.251±0.055	0.019	0.460

trend maps for settlements across the basin, especially for 19 settlements examined in greater detail (Table 1).

Regression analysis. To implement this analysis at the basin scale, we used a time series of Landsat satellite images acquired in July and August (typically the hottest months) from 1984 to 2024. Cloud-covered pixels and their shadows were masked to ensure data consistency and reliability.

Time series analysis identifies the characteristic features of the evolution (dynamics) of atime series, which necessarily have a functional dependence on various factors influencing the system. Time series dynamics comprises several components, which are manifestations of multiple effects on the system and are integral to the time series. The principal elements shaping the dynamics of the time series are trend, cyclical, seasonal, and random fluctuations [Altman, Krzywinski, 2015].

A trend is the general nature of a time series's evolution, specifically the direction of its change over a long period or throughout the analyzed period. Often, the time series trend is described by a fundamental mathematical dependency (linear, quadratic, exponential, or some other). Cyclical fluctuations are rapid changes in the dynamics of a series, characterized by rising and falling phases. Seasonal fluctuations occur over a day or a season (seasons). Random fluctuations are unsystematic fluctuations of high frequency and low amplitude, associated with the constant influence on the system of various events and processes on the studied quantity [Hemati et al., 2021].

The key result of the time series analysis is a temperature trend, which shows the distribution of annual temperature increases for the studied area over the analyzed period. Correct preparation of thermal images is particularly crucial to avoid miscalculations distorted by the low temperatures of clouds and their shadows. Unfortunately, cloudiness interferes with obtaining the needed accuracy of prediction. Nevertheless, the process of masking and further counting pixel cover might clarify whether you can rely on this result. In other words, ensure that the pixels of images in the collection have a NaN (Not a Number) value for the best results. This image enables the localization of temperature trends for each pixel in the studied area, thereby describing the long-term changes that occurred in the thermal regime during the experimental period.

A precise spatial alignment of the images allows you to describe the physical characteristics of the earth's surface in a particular area for all the years for which the data from the space survey was processed without spatial distortions. The accumulation of indicator values in each pixel allows you to form a sample for all years and calculate a regression dependence that will demonstrate the growth of the indicator value over the entire experimental period and the regression calculation for each spatial cell of the experimental area presented in the image allows you to obtain the spatial distribution of the indicator dynamics within the entire research area.

Linear regression, in this case, represents an estimate of the linear dependence of the indicator on time and can represent the landscape changes that occurred during the experimental period. A linear, univariate regression is represented below:

$$R(x, y) = xa + b, \qquad (4)$$

where x is the independent variable (year), y is the dependent variable (temperature), a is the slope (angular coefficient), indicating the rate of change, b is the intercept, representing the starting value at year zero.

Although non-parametric methods, such as the Mann-Kendall test [Mann, 1945; Kendall, 1975], are widely used to detect trends due to their robustness to non-normal data distributions and outliers, we employ linear regression as the primary analytical tool. This choice is motivated by the need to quantify not only the direction but also the magnitude (slope) of temperature change over time, providing interpretable coefficients directly related to the rate of change. Furthermore, preliminary analysis confirmed that the LST time series exhibited near-linear temporal behavior with minimal autocorrelation, making regression analysis both appropriate and ef-

ficient for the dataset under consideration.

Results and discussion. In this study, the dependent variable is the value of each indicator in each pixel for a specific year, and the independent variable is the year in which the image data were obtained. Each enabled period in Fig. 4 has its deviation from the underlying straight-line model. The value is estimated by equation (4) but with the addition of an «error» term, which is the distance between the period and the intersection with the line on the parallel y-axis.

The most common method of calculating the regression dependence is the method of least squares, which simplifies the task of finding the coefficients of linear dependence that minimize the value of the function of two variables, a and b. That is, with the data a and b, the sum of the squares of the deviations of the experimental data from the found straight line will be the smallest.

To construct the spatial distribution of the long-term dynamics of the obtained temperatures, the gradient of the calculated regression or the angular coefficient is used, which, in its physical essence, represents the average annual increase in the value of the indicator.

For the area pinned at the pixel of the 2000th row and 750th column, the equation y=0.0732x+25.8692 is the regression dependence, where 0.0732 is the angular regression coefficient, which represents the average annual increase of the temperature indicator.

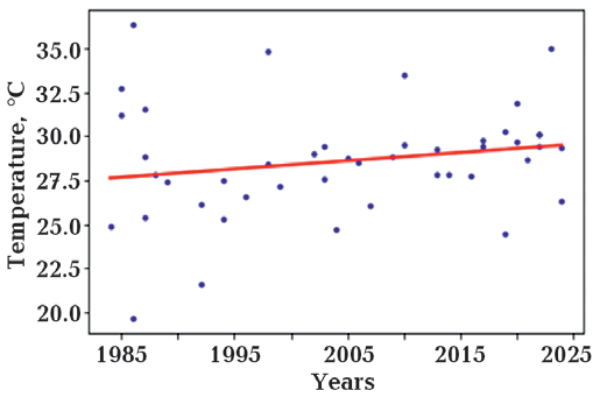

Fig. 4. A representative example of deriving a regression dependency from a temporal sequence of indicator values (red line — linear regression, blue points — temperature for the corresponding years).

Fig. 5 shows the mean land surface temperature since 1984. This map utilizes color gradients to represent temperature.

Fig. 6 illustrates the annual increase in land surface temperature for the same period. The map utilizes a color gradient to represent temperature changes, where blue represents negative values. The increments increase in steps of 0.2 degrees Celsius.

Combining average temperature data with annual increments for the period from 1984 to 2024 enables a deeper understanding of the spatiotemporal dynamics of climate change at both local and regional scales. While the average temperature reflects the overall thermal state of a territory, the annual increment indicates the rate and direction of change, which is particularly important for identifying warming trends or local anomalies.

The results were obtained through a two-stage process. In the first stage, raster data were prepared and analyzed using the cloud-based platform Google Earth Engine. A key advantage of this environment is its capability to automate the export of georeferenced data in the GeoTIFF format while encoding the image acquisition date directly into the file name. This functionality enabled the automation of the second stage, which involved calculating the annual increment of land surface temperature through regression analysis using a Python-based script. A distinctive feature of this script is its universality — it automatically processes all raster files located in the same directory, extracts temporal metadata from file names, and performs time-series regression. Together, these two stages constitute an integrated workflow for calculating annual temperature trends from satellite imagery, specifically Landsat data.

The urban and rural settlements presented in Table 1 exhibit positive temperature trends. The table contains statistical data on the maximum, minimum, and mean temperature increase, as well as the standard deviation (SD) with its range. This highlights the importance of urban greening — the process of increasing vegetation cover through the planting of grass, trees, and other plants. Greening initiatives can play a critical role in mitigating the

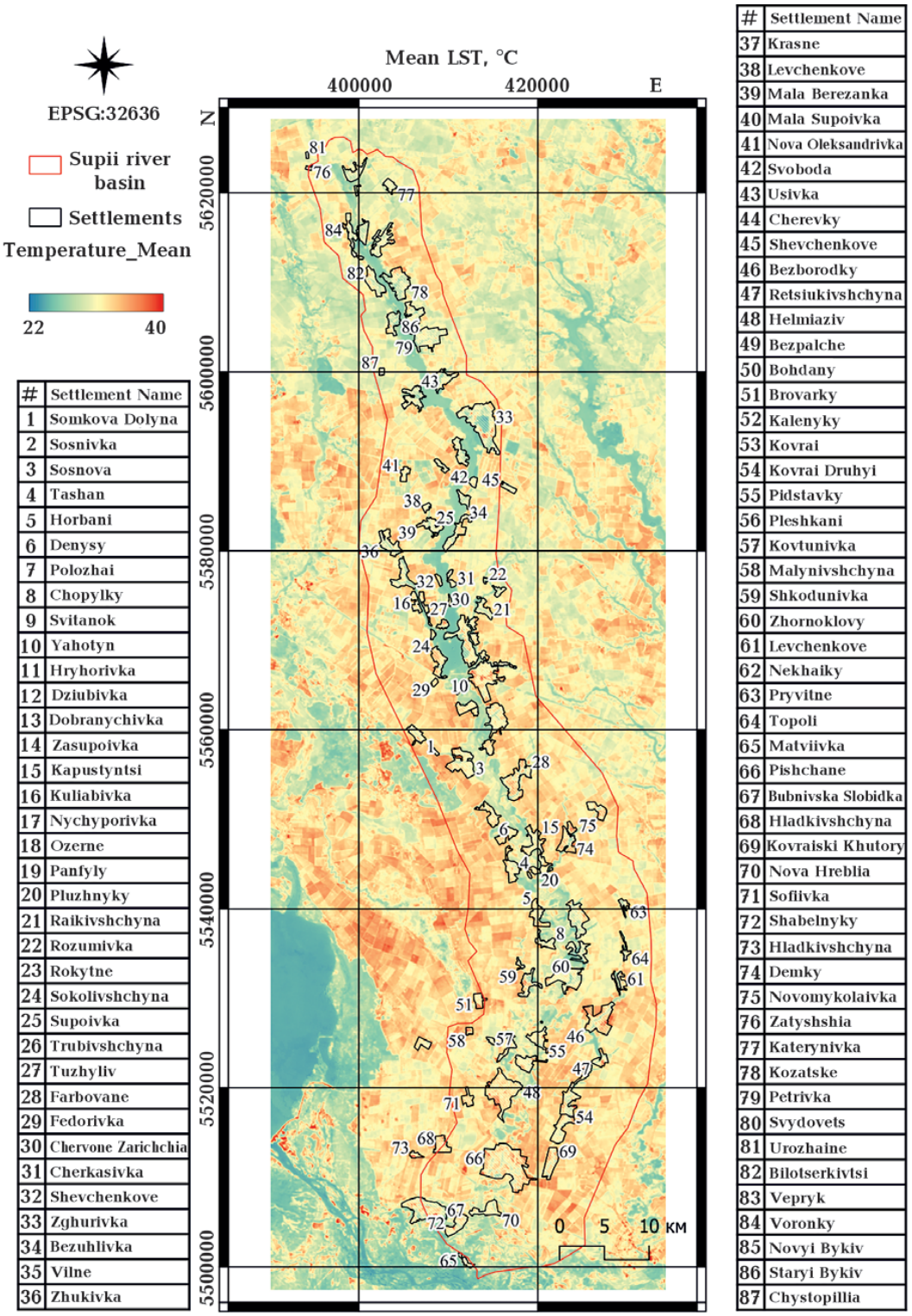

#	Settlement Name
1	Somkova Dolyna
2	Sosnivka
3	Sosnova
4	Tashan
5	Horbani
6	Denysy
7	Polozhai
8	Chopylky
9	Svitanok
10	Yahotyn
11	Hryhorivka
12	Dziubivka
13	Dobranychivka
14	Zasupoivka
15	Kapustyntsi
16	Kuliabivka
17	Nychyporivka
18	Ozerne
19	Panfyly
20	Pluzhnyky
21	Raikivshchyna
22	Rozumivka
23	Rokytne
24	Sokolivshchyna
25	Supoivka
26	Trubivshchyna
27	Tuzhyliv
28	Farbovane
29	Fedorivka
30	Chervone Zarichchia
31	Cherkasivka
32	Shevchenkove
33	Zghurivka
34	Bezuhlivka
35	Vilne
36	Zhukivka

#	Settlement Name
37	Krasne
38	Levchenkove
39	Mala Berezanka
40	Mala Supoivka
41	Nova Oleksandrivka
42	Svoboda
43	Usivka
44	Cherevky
45	Shevchenkove
46	Bezborodky
47	Retsiukivshchyna
48	Helmiaziv
49	Bezpalche
50	Bohdany
51	Brovarky
52	Kalenyky
53	Kovrai
54	Kovrai Druhyi
55	Pidstavky
56	Pleshkani
57	Kovtunivka
58	Malynivshchyna
59	Shkodunivka
60	Zhornoklovy
61	Levchenkove
62	Nekhaiky
63	Pryvitne
64	Topoli
65	Matviivka
66	Pishchane
67	Bubnivska Slobidka
68	Hladkivshchyna
69	Kovraiski Khutory
70	Nova Hreblia
71	Sofiivka
72	Shabelnyky
73	Hladkivshchyna
74	Demky
75	Novomykolaivka
76	Zatyshshia
77	Katerynivka
78	Kozatske
79	Petrivka
80	Svydovets
81	Urozhaine
82	Bilotserkivtsi
83	Vepryk
84	Voronky
85	Novyi Bykiv
86	Staryi Bykiv
87	Chystopillia

Fig. 5. Mean land surface temperature of Supii River basin from 1984 to 2024.

urban heat island effect and enhancing local climate resilience.

For example, in Zhurivka, the presence of a large national park and only a few industrial facilities contributes to the lowest mean annual LST increment.

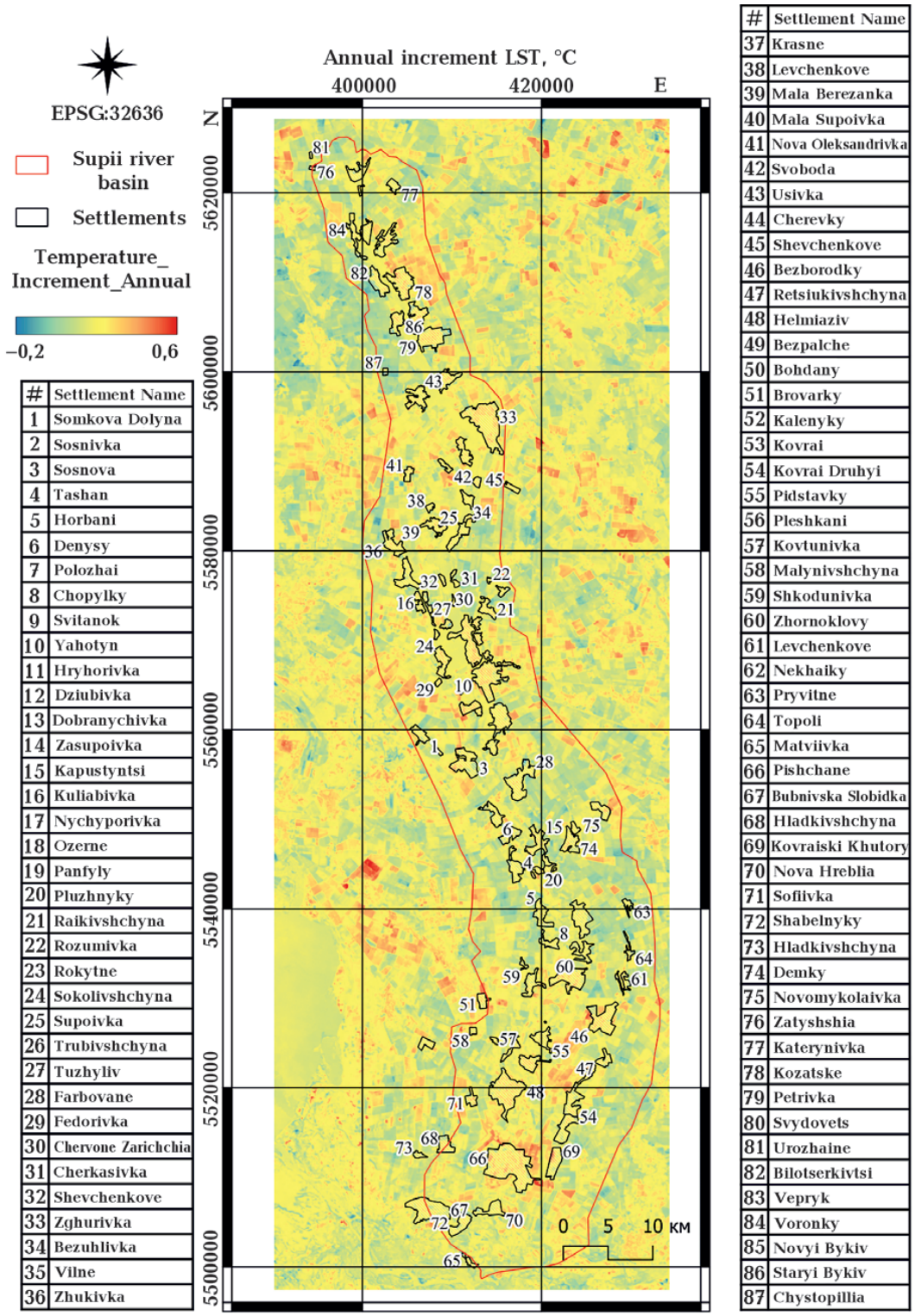

#	Settlement Name
1	Somkova Dolyna
2	Sosnivka
3	Sosnova
4	Tashan
5	Horbani
6	Denysy
7	Polozhai
8	Chopylky
9	Svitanok
10	Yahotyn
11	Hryhorivka
12	Dziubivka
13	Dobranychivka
14	Zasupoivka
15	Kapustyntsi
16	Kuliabivka
17	Nychyporivka
18	Ozerne
19	Panfyly
20	Pluzhnyky
21	Raikivshchyna
22	Rozumivka
23	Rokytne
24	Sokolivshchyna
25	Supoivka
26	Trubivshchyna
27	Tuzhyliv
28	Farbovane
29	Fedorivka
30	Chervone Zarichchia
31	Cherkasivka
32	Shevchenkove
33	Zghurivka
34	Bezuhlivka
35	Vilne
36	Zhukivka

#	Settlement Name
37	Krasne
38	Levchenkove
39	Mala Berezanka
40	Mala Supoivka
41	Nova Oleksandrivka
42	Svoboda
43	Usivka
44	Cherevky
45	Shevchenkove
46	Bezborodky
47	Retsiukivshchyna
48	Helmiaziv
49	Bezpalche
50	Bohdany
51	Brovarky
52	Kalenyky
53	Kovrai
54	Kovrai Druhyi
55	Pidstavky
56	Pleshkani
57	Kovtunivka
58	Malynivshchyna
59	Shkodunivka
60	Zhornoklovy
61	Levchenkove
62	Nekhaiky
63	Pryvitne
64	Topoli
65	Matviivka
66	Pishchane
67	Bubnivska Slobidka
68	Hladkivshchyna
69	Kovraiski Khutory
70	Nova Hreblia
71	Sofiivka
72	Shabelnyky
73	Hladkivshchyna
74	Demky
75	Novomykolaivka
76	Zatyshshia
77	Katerynivka
78	Kozatske
79	Petrivka
80	Svydovets
81	Urozhaine
82	Bilotserkivtsi
83	Vepryk
84	Voronky
85	Novyi Bykiv
86	Staryi Bykiv
87	Chystopillia

Fig. 6. Annual increment of the land surface temperature of Supii River basin from 1984 to 2024.

Other settlements along the Supii River demonstrate varying degrees of LST increase, reflecting differences in land use, urbanization intensity, and vegetation cover. Notably, Kozatske and Pishchane exhibit the highest mean annual LST increments (0.251 °C and

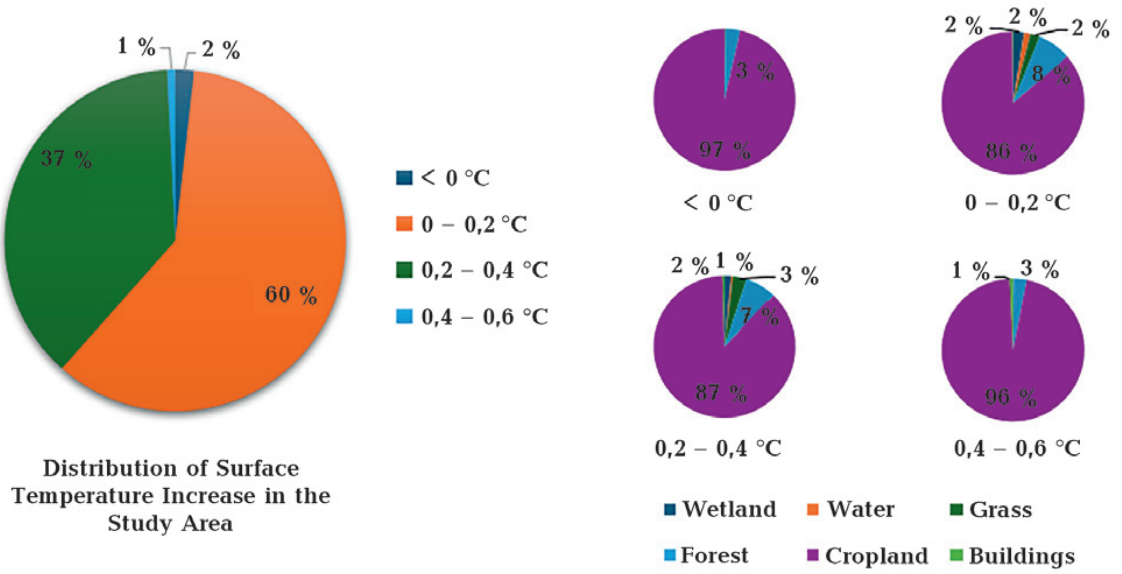

Fig. 7. Surface temperature increase by land use type in the study area.

0.250 °C, respectively), indicating intensified surface warming that may be linked to reduced vegetation or increased non-permeable surfaces.

Yahotyn, the largest urban center in the basin, shows a significant maximum increment of 0.501 °C and a broad temperature range of 0.634 °C. This variability suggests the presence of both densely developed zones and vegetated or water-rich areas, possibly moderating the overall mean despite high local anomalies.

Bezborodky and Novyi Bykiv also show relatively high mean increments (0.234 °C and 0.229 °C) and broad ranges, pointing to considerable spatial heterogeneity, likely influenced by mixed land use, including agriculture and infrastructure.

Settlements like Tashan, Horbani, and Nekhaiky display moderate increments with lower standard deviations, suggesting more homogeneous thermal behavior, likely due to consistent land cover and limited urban expansion.

Interestingly, Petrivka and Farbovane exhibit some negative minimum values (–0.137 °C, –0.150 °C), which may reflect zones of increased vegetation or seasonal water bodies that have a cooling effect. However, their wide ranges and relatively high standard deviations imply local areas with intensified heat, possibly due to land misuse or exposed soils.

These results underscore the need for differentiated land management strategies, particularly in settlements where thermal dynamics point to unsustainable practices or vulnerable ecosystems. Integrating thermal data with normalized vegetation or moisture indices could enhance the precision of such assessments and support progress toward Sustainable Development Goals (SDGs) related to climate action, sustainable cities, and land degradation neutrality.

Irregular fluctuations in the regression analysis (spikes in increments outside urban areas) are associated with agricultural activity and the use of different crop types. Such unsustainable land use — often corresponding to the hottest surface areas — contributes to land degradation. To examine this relationship in more detail, we used the results of land use classification [Marhes, 2023], which formed the basis for comparing temperature increases across different land use types (Fig. 7 and Table 2).

Of particular concern are peatland areas, which are becoming increasingly vulnerable due to the rising risk of fire. This vulnerability is driven by intensive evapotranspiration

Table 2. Distribution of LST Increase by Land Use Type, %

Type	<0 °C	0—0.2 °C	0.2—0.4 °C	0.4—0.6 °C
Wetland	0.186	2.480	1.513	0.000
Water	0.007	1.517	0.416	0.000
Grass	0.094	2.109	3.114	0.186
Forest	3.285	7.560	7.146	2.887
Cropland	96.420	86.170	87.327	96.138
Buildings	0.007	0.165	0.485	0.789

under elevated air temperatures. Further investigation of these zones will support the development of more precise adaptation and management recommendations [Lischenko et al., 2022; Lubskyi et al., 2023].

Cloud cover did not significantly affect the results, as all pixels identified as clouds or cloud shadows were excluded from the regression analysis through prior masking.

The methodology used in this study can be extended to other regions with comparable climatic and land use conditions, offering potential for large-scale environmental monitoring. Future research should focus on improving the spatial resolution of emissivity datasets, integrating additional environmental variables such as soil moisture and albedo, and validating results with in-situ thermal measurements. Furthermore, the proposed approach has potential applications in climate change impact assessment, agricultural drought monitoring, and land degradation studies, supporting evidence-based decision-making and sustainable land management practices.

Conclusions. Based on the obtained regression coefficients, long-term landscape changes within the experimental area were identified, including the dynamics of increasing land surface temperature values. These changes were quantified for each element of the shared pixel grid.

In this study, the average temperature and annual rate of increase over the past 40 years were calculated. This approach enabled the identification of primary sources of thermal pollution as well as a detailed analysis of temperature increments within both urban and rural settlements.

Integratingthese data with normalized indices can be valuable for related studies. For example, combining temperature data with the Normalized Difference Water Index (NDWI) can help reveal the relationship between temperature and moisture content.

The only limitation of this approach is the relatively small amount of available data. The greater the number of raster images used, the more reliable the statistical analysis and subsequent predictions will be.

References

Altman, N., & Krzywinski, M. (2015). Simple linear regression. *Nature Methods, 12*(11), 999—1000. https://doi.org/10.1038/nmeth.3627.

Bala, R., Prasad, R., Yadav, V.P., & Sharma, J. (2018). A comparative study of land surface temperature with different indices on heterogeneous land cover using Landsat 8 data. *International Archives of the Photogrammetry, Remote Sensing and Spatial Information Sciences, 42*(5), 389—394. https://doi.org/10.5194/isprs-archives-xlii-5-389-2018.

Bowman, A.W., & Azzalini, A. (1997). *Applied smoothing techniques for data analysis: The kernel approach with S-Plus illustrations*. Oxford University Press, 191 p.

Brockwell, P.J., & Davis, R.A. (Eds.). (2002). *Introduction to time series and forecasting*. Springer. https://doi.org/10.1007/b97391.

Chander, G., Markham, B.L. & Helder, D.L. (2009). Summary of current radiometric calibration coefficients for Landsat MSS, TM, ETM+, and

EO-1 ALI sensors. *Remote Sensing of Environment, 113*(5), 893—903. https://doi.org/10.1016/j.rse.2009.01.007.

Chatfield, C. (2000). *Time-series forecasting*. Chapman & Hall/CRC. https://doi.org/10.1201/9781420036206.

Cohn, P.M. (1994). *Elements of linear algebra*. Chapman & Hall/CRC. ISBN 9780412552809.

Derii, M.M. (2007). Report on the geological survey of the subsurface: Geological structure and minerals of the confluence of the Trubizh and Supii rivers (Book 1). State Geological Service of Ukraine.

Draper, N.R., & Smith, H. (1998). *Applied regression analysis* (3rd ed.). John Wiley & Sons.

Filipovych, V.Ye., & Shevchuk, R.M. (2018). Satellite technology for determining the heat load on the city in summer and ways to overcome it through green planning. *Conference:Sustainable cities: Implementing green planning, design and construction ideas in Ukraine*. https://doi.org/10.13140/RG.2.2.17113.08807.

Hemati, M., Hasanlou, M., Mahdianpari, M., & Mohammadimanesh, F. (2021). A Systematic Review of Landsat Data for Change Detection Applications: 50 Years of Monitoring the Earth. *Remote Sensing, 13*, 1—33. https://doi.org/10.3390/rs13152869.

Ismaila, A.-R.B., Muhammed, I., & Adamu, B. (2023). A spatial regression approach to modeling urban land surface temperature. *MethodsX, 10*, 1025. https://doi.org/10.1016/j.mex.2023.1025.

Kendall, M.G. (1975). *Rank correlation methods* (4th ed.). Charles Griffin.

Li, X., Wang, Y., & Wu, C. (2018). «Regression-then-Fusion» or «Fusion-then-Regression»? A theoretical analysis for generating high spatiotemporal resolution land surface temperatures. *Remote Sensing, 10*(9), 1382. https://doi.org/10.3390/rs10091382.

Lischenko, L., Shevchuk, R., & Filipovych, V. (2022). The technique for satellite monitoring of peatlands in order to determinate their fire hazard and combustion risks. *Ukrainian Journal of Remote Sensing, 9*(1), 23—32. https://doi.org/10.36023/ujrs.2022.9.1.210 (in Ukrainian).

Lubskyi, M., Khyzhniak, A., Piestova, I., & Orlenko, T. (2025). Land surface emissivity estimation technique based on NDVI/ASTER GED data correlation. *18th International Conference Monitoring of Geological Processes and Ecological Condition of the Environment, 2025* (pp. 1—5). https://doi.org/10.3997/2214-4609.2025510040.

Lubskyi, M., Orlenko, T., Piestova, I., Andreiev, A., & Lysenko, A. (2023). Evaluation of indicators for desertification risk assessment of Oleshky sands desertification based on Landsat data time series. *Ukrainian Journal of Remote Sensing, 10*(1), 17—28. https://doi.org/10.36023/ujrs.2023.10.1.229 (in Ukrainian).

Lyalko, V.I., Filipovich, V.E., Lischenko, L.P., Pazynych, N.V., Teremenko, A.N., & Krylova, A.B. (2016). Remote sensing monitoring of historical centre of Kyiv for reducing risks from disasters at world heritage properties. *Journal of the Japanese Geotechnical Society Special Publication, 2*(78), 2671—2675. https://doi.org/10.3208/jgssp.TC301-04.

Management plan of the Dnieper river basin: Part 1 (2025—2030). (2021). Ministry of Environmental Protection and Natural Resources of Ukraine, 422 p. Retrieved from https://davr.gov.ua/fls18/DNIPRO4.pdf.

Mann, H.B. (1945). Nonparametric tests against trend. *Econometrica, 13*(3), 245—259. https://doi.org/10.2307/1907187.

Marhes, S.V. (2023). Research of the Supiya River Valley as a Link of the Emerald Network of Europe Using GIS Technologies and Remote Sensing Methods. In S.O. Dovgy (Ed.), *Information and Communication Technologies for Victory and Recovery* (pp. 193—195). Kyiv: Yuston Publishing House (in Ukrainian).

Stankevich, S.A., Filipovich, V.E., Lubsky, N.S., Krylova, A.B., Kritsuk, S.G., Brovkina, O.V., Gornyy, V.I., & Tronin, A.A. (2015). Intercalibration of methods for land surface thermodynamic temperature retrieval inside urban areas by thermal-infrared satellite imaging. *Ukrainian Journal of Remote Sensing,* (7), 12—21 (in Russian).

Valor, E., & Caselles, V. (1996). Mapping land surface emissivity from NDVI: Application to European, African, and South American areas. *Remote Sensing of Environment, 57*(3), 167—184. https://doi.org/10.1016/0034-4257(96)00039-9.

Yu, X., Guo, X., & Wu, Z. (2014). Land surface

temperature retrieval from Landsat 8 TIRS-Comparison between radiative transfer equation-based method, split window algorithm and single channel method. *Remote Sensing*, *6*(10), 9829—9852. https://doi.org/10.3390/rs6109829.

Zhang, Y., & Li, Z. (2020). Modelling future land surface temperature: A comparative analysis between parametric and non-parametric methods. *Sustainability*, *12*(18), 8195. https://doi.org/10.3390/su12188195.

Просторово-часовий аналіз динаміки поверхневих температур басейну річки Супій із застосуванням регресійного аналізу

С.В. Маргес, В.Є. Філіпович, М.С. Лубський, 2025

Державна установа «Центр аерокосмічних досліджень Землі ІГН НАН України», Київ, Україна

У дослідженні представлено підхід до оцінки просторових і часових змін температури поверхні землі, зокрема річного приросту температури. Район дослідження охоплює басейн річки Супій, яка перетинає Чернігівську, Київську та Черкаську області і впадає в Дніпро. Для цієї місцевості характерні інтенсивне сільськогосподарське використання земель, слабка водонасиченість водоносного горизонту, низька якість підземних вод і тривалі посушливі періоди.

Дані про температуру за липень та серпень було отримано з архівів місій Landsat з 1984 і до 2024 р. Обґрунтовано необхідність перерахунку температурних знімків Landsat на основі випромінюваної здатності, оскільки їхній продукт L2 може мати пікселі без інформації. Для підвищення точності аналізу зображення були очищені від пікселів, спотворених хмарами та їхніми тінями.

На основі відфільтрованих даних проведено аналіз часових рядів, основна мета якого — виявити характерні риси еволюції температурних змін у динаміці, що є результатом дії комплексу природних та антропогенних чинників. Завдяки чіткому просторовому вирівнюванню знімків вдалося забезпечити достовірність розрахунків фізичних характеристик земної поверхні в межах досліджуваної території для кожного року. Для кожного пікселя було застосовано метод простої лінійної регресії, що дало змогу визначити кутовий коефіцієнт — градієнт зміни температури, який у цьому контексті відображає середньорічний приріст показника.

Результати подано у вигляді просторових індексів річного приросту температури в басейні річки Супій, з акцентом на окремі населені пункти, де спостерігається переважання позитивних трендів, і розподілом за землекористуванням. Це дозволило оцінити, де і наскільки критичною може бути ситуація у найближчі роки за умов подальшого підвищення температури. Як один із можливих підходів до пом'якшення наслідків глобального потепління, запропоновано активне озеленення міських і сільських територій, особливо у межах великих територіальних громад.

Ключові слова: лінійна регресія, часові ряди, поверхнева температура, річний приріст, глобальне потепління.